THE JOURNAL OF BIOLOGICAL CHEMISTRY Vol. 278, No. 37, Issue of September 12, pp. 35564–35573, 2003

Printed in U.S.A.

Structure and Inhibitory Effects on Angiogenesis and Tumor Development of a New Vascular Endothelial Growth Inhibitor*[S]

Received for publication, April 29, 2003, and in revised form, June 30, 2003
Published, JBC Papers in Press, July 1, 2003, DOI 10.1074/jbc.M304435200

Lior Zilberberg‡§, Svetlana Shinkaruk¶, Olivier Lequin‖, Benoit Rousseau‡, Martin Hagedorn‡, Francesco Costa‡‡, Dario Caronzolo‡‡, Maurice Balke‡, Xavier Canron‡, Odile Convert‖, Georges Laïn¶, Karine Gionnet¶, Mario Gonçalvès¶, Mireille Bayle¶, Lorenzo Bello‡‡, Gerard Chassaing‖, Gérard Deleris¶, and Andreas Bikfalvi‡§§§**

From the ‡Molecular Angiogenesis Laboratory (INSERM E 0113), Université de Bordeaux 1, 33405 Talence, ¶Groupe de Chimie Bio-Organique (INSERM U 577), Université Victor Segalen Bordeaux 2, 33076 Bordeaux Cedex, ‖Structure et Fonction de Molécules Bioactives (UMR 7613 CNRS-Université Paris 6), Université Pierre et Marie Curie, 4 Place Jussieu, 75252 Paris Cedex 05, France, and ‡‡Neurosurgery, Department of Neurological Sciences, University of Milano, Ospedale Maggiore Policlinico, Istituto di Ricovero e Cura a Carattere Scientifico, 20122 Milan, Italy

Blocking angiogenesis is an attractive strategy to inhibit tumor growth, invasion, and metastasis. We describe here the structure and the biological action of a new cyclic peptide derived from vascular endothelial growth factor (VEGF). This 17-amino acid molecule designated cyclopeptidic vascular endothelial growth inhibitor (cyclo-VEGI, CBO-P11) encompasses residues 79–93 of VEGF which are involved in the interaction with VEGF receptor-2. In aqueous solution, cyclo-VEGI presents a propensity to adopt a helix conformation that was largely unexpected because only β-sheet structures or random coil conformations have been observed for macrocyclic peptides. Cyclo-VEGI inhibits binding of iodinated $VEGF_{165}$ to endothelial cells, endothelial cells proliferation, migration, and signaling induced by $VEGF_{165}$. This peptide also exhibits anti-angiogenic activity *in vivo* on the differentiated chicken chorioallantoic membrane. Furthermore, cyclo-VEGI significantly blocks the growth of established intracranial glioma in nude and syngeneic mice and improves survival without side effects. Taken together, these results suggest that cyclo-VEGI is an attractive candidate for the development of novel angiogenesis inhibitor molecules useful for the treatment of cancer and other angiogenesis-related diseases.

Angiogenesis takes place during embryonic development and in the adult during wound healing and the female ovulatory cycle. In pathological states, angiogenesis is observed during solid tumor growth and metastasis, diabetic retinopathy, and chronic inflammatory disorders. A number of angiogenic regulators such as vascular endothelial growth factors (VEGFs),[1] fibroblast growth factors (FGFs), and angiopoietins have been identified (1–4).

VEGFs are endothelial cell mitogens *in vitro* and also stimulate angiogenesis *in vivo* (2, 5, 6). VEGF exerts its biological effects through high affinity binding to two tyrosine kinase receptors, VEGFR1 (Flt-1) and VEGFR2 (kinase domain receptor), which are expressed in most vascular endothelial cells (6–8). VEGF is expressed in a large number of human tumor types (9, 10). Clinical studies have documented the importance of VEGF in human cancers. As an example, VEGF is increased in the plasma of cancer patients and is correlated with response to chemotherapy (11, 12). In growing tumors, VEGF expression is up-regulated by hypoxia, growth factors, and oncogenes (6, 13).

Antagonizing VEGF has shown to inhibit tumor development *in vivo*. Different strategies have been designed to inhibit VEGF function. These include monoclonal neutralizing antibodies (14), dominant-negative mutants of the VEGF receptor-2 (VEGFR2) (15), antisense oligonucleotides (16), anti-VEGFR2 antibodies (17), blockers of VEGFR2 tyrosine phosphorylation (18), VEGF-toxin conjugates (19), antagonistic VEGF mutants (20), peptides that interfere with VEGF/VEGFR interactions (21–25), and decoy-soluble receptors (26).

Relevant regions of VEGF important for its binding on VEGFR2 and VEGFR1 have been investigated by structural and mutagenesis studies (27–29). Some of the residues important for the interaction between VEGF and kinase domain receptor are clustered within region 79–93 of VEGF which

* This work was supported in part by grants from la Ligue Nationale Contre le Cancer ("Equipe Labelisée"), the Ministère de la Recherche, the INSERM, by the Conseil Régional d'Aquitaine (to A. B. and to G. D.), by grants from Associazione Italiana Ricerca sul Cancro, "Fondazione Monzino," Milano, Compagnia di San Paolo, Progetto Oncologia, Torino, Italy (to L. B.), and by grants from la Ligue Contre le Cancer (to G. D.). The costs of publication of this article were defrayed in part by the payment of page charges. This article must therefore be hereby marked "*advertisement*" in accordance with 18 U.S.C. Section 1734 solely to indicate this fact.

[S] The on-line version of this article (available at http://www.jbc.org) contains Tables S1–S3.

§ Supported by the "Association pour la Recherche Contre le Cancer."

** Supported by the "Fédération des Avaugles et Handicapés Visuels de France."

§§ To whom correspondence should be addressed: INSERM E 0113, Molecular Angiogenesis Laboratory, Université de Bordeaux 1, 33405 Talence, France. Fax: 33-5-40-00-87-05; E-mail: a.bikfalvi@croissance.u-bordeaux.fr.

[1] The abbreviations used are: VEGF, vascular endothelial growth factor; FGF-2, fibroblast growth factor-2; PDGF-BB, platelet-derived growth factor-BB; cyclo-VEGI, cyclo-vascular endothelial growth inhibitor; CAM, chorioallantoic membrane; VEGFR, vascular endothelial growth factor receptor; BAE, bovine aortic endothelial; BCE, bovine capillary endothelial; CHO, Chinese hamster ovary; ERK1,2, extracellular signal-regulated kinases 1 and 2; HUVEC, human umbilical vein endothelial cell; PBS, phosphate-buffered saline; CSD, chemical shift deviation; HSQC, heteronuclear single quantum correlation spectroscopy; TFE, 2,2,2-trifluoroethanol; DMEM, Dulbecco's modified Eagle's medium; FBS, fetal bovine serum; MAP, mitogen-activated protein; HSPG, heparan sulfate proteoglycan; Fmoc, *N*-(9-fluorenyl)methoxycarbonyl; NOE, nuclear Overhauser effect; NOESY, nuclear Overhauser effect spectroscopy; EC, endothelial cell; TOCSY, total correlation spectroscopy; HMPB, total correlation spectroscopy; BHA, butylated hydroxyanisole; HSPGs, heparan sulfate proteoglycans.

forms a β-hairpin, Arg^{82}, Lys^{84}, and His^{86} being key residues (27). Based on these structural and mutagenesis studies, a number of cyclic and linear peptides have been synthesized. One of the most potent compound was the cyclic peptide CBO-P11 (D-Phe-Pro^{79-93}) designated herein cyclopeptidic vascular endothelial growth inhibitor (cyclo-VEGI).[2] In the present report, we determined the structural features of this peptide and characterized its biological properties. We show that this peptide adopts an unexpected three-dimensional structure and is able to inhibit critical steps of angiogenesis. Moreover, this peptide inhibits the growth of both established human intracranial and syngeneic glioma in mice.

EXPERIMENTAL PROCEDURES

Structural Analysis of Cyclo-VEGI (CBO-P11)

NMR Spectroscopy—NMR samples were prepared at a 2 mM peptide concentration in water or in mixtures of TFE-d_3/water containing 10% D_2O. All NMR spectra were recorded on Bruker Avance spectrometers operating at a ^1H frequency of 500 MHz and were processed with the Bruker XWINNMR program. One-dimensional spectra were acquired over 16 K data points using a spectral width of 5000 Hz and a reference to internal sodium 3-trimethylsilyl-(2,2,3,3-$^2H_4$)propionate at 0 ppm. Solvent suppression was achieved by presaturation during the relaxation delay (1.5 s) or with a WATERGATE sequence using pulsed field gradients (30). Proton assignments were obtained at 288 and 298 K from the analysis of TOCSY (20- and 80-ms isotropic mixing times) and NOESY (150-, 200-, or 300-ms mixing times) spectra (31, 32). Typically, two-dimensional data were collected with 400–600 t_1 increments and 2048 data points in t_2, over a spectral width of 6000 Hz in both dimensions. Prior to Fourier transformation in t_2 and t_1, the time domain data were multiplied by a $\pi/3$ shifted square sinebell function and zero-filled. Base-line distortions were corrected with a fifth-order polynomial function. ^1H-^{13}C HSQC experiments were acquired using pulsed field gradients for coherence selection (33). The chemical shift deviations of H^a and C^a were calculated using random coil values reported in water (34). The temperature gradients of the amide proton chemical shifts were derived from a series of TOCSY spectra recorded at different temperatures (from 283 to 303 K). The resonances assignments are listed in Tables S1–S3 in the Supplemental Material.

Structure Calculation—Interproton distance restraints were derived from the analysis of NOESY spectra. NOE cross-peaks were categorized as strong, medium, and weak and converted into distance ranges of 0.18–0.28, 0.18–0.38, and 0.18–0.5 nm, accordingly. Pseudoatoms were introduced for distances involving methyl protons and non-resolved methylene protons, and upper limits were corrected appropriately (35). The ϕ angle of L-amino acid residues was restrained to negative values because all these residues did not exhibit strong intraresidual $d\alpha N$ NOEs. Structures were calculated using InsightII version 98.0 and Discover (Accelrys, San Diego, Inc.), running on SGI O2 R10000 workstations, and AMBER forcefield (36). The simulated annealing protocol first comprised 15 ps of dynamics at 1000 K during which the force constants of the distance and dihedral restraint terms were gradually increased. The non-bond interaction, defined by a simple quartic repulsive potential, was slowly increased during the next 10 ps of dynamics. Finally, the structures were cooled from 1000 to 0 K over 25 ps. The structures were then minimized by steepest descent and conjugated gradient algorithms, using a Lennard-Jones potential for the van der Waals interaction and a distance-dependent dielectric screening of $4r$ for the electrostatic term.

Growth Factors and Peptides Synthesis

Recombinant human FGF-2 was kindly provided by Dr. Hervé Prats (INSERM U397, Toulouse, France) and stored in sterile, double-distilled water at −80 °C. Recombinant human $VEGF_{165}$ was produced in insect cells and purified as described elsewhere (37, 38). Human $VEGF_{165}$-encoding baculovirus was a kind gift of Dr. Jean Plouët (Institut de Pharmacologie et de Biologie Stucturale, UMR 5089, Toulouse, France). CBO-P11 (cyclo-VEGI) (*D*FPQIMRIKPHQGQHIGE) and linear control CBO-P14 (PQIMRIKPHQGQHIGE) peptides were synthesized by Fmoc/*t*-butyl batch solid phase synthesis on an Applied Biosystems 430A automated peptide synthesizer. For preparation of protected peptide fragments, pre-loaded acid-labile 2-chlorotrityl resins (H-His(Trt)^2-ClTrt and H-Ile^2-ClTrt resin) or HMPB-BHA resins based on BHA polystyrene functionalized with Rink's 4-hydroxymethyl-3-methoxyphenoxybutanoic acid linker (Fmoc-Gly-HMPB-BHA resin) were utilized. Subsequent Fmoc amino acids were coupled using a 4-fold excess of amino acids activated as HOBt ester by means of DCC. The crude linear protected peptides were analyzed by reverse phase high pressure liquid chromatography on a Lichrosorb RP-18 column (Merck) and purified on semi-preparative high pressure liquid chromatography. Cyclization of the protected linear precursor (head-to-tail) was performed by Fmoc/*t*-butyl/allyl strategy.[2]

Cell Culture

Bovine capillary endothelial (BCE) cells were a kind gift of Dr. Daniel B. Rifkin (New York University Medical Center, New York). Bovine aortic endothelial (BAE) cells were from Dr. Georg Breier (Department of Molecular Biology, Max-Planck-Institut für physiologische und Klinische Forschung, Bad Nauheim, Germany). All endothelial cells were grown at 37 °C, 5% CO_2 in DMEM containing 10% newborn calf serum, 2 mM L-glutamine, and 50 IU/ml penicillin, 50 IU/ml streptomycin antibiotics and were used up to passage 25. BCE cells were grown in the presence of 2 ng/ml FGF-2. CHO-VEGFR2 and CHO-VEGFR1 cells were a kind gift of Dr. J. Plouët (GDR CNRS 1927 "Angiogenèse," Toulouse, France). CHO-VEGFR2 and CHO-VEGFR1 were grown in DMEM supplemented with 10% fetal calf serum, 2 mM L-glutamine, 1% non-essential amino acids and antibiotics (Invitrogen). Balb3T3 were grown in DMEM supplemented with 10% FBS, 2 mM L-glutamine, and antibiotics. U87 human glioma cells (ATCC) were grown in minimum Eagle's α-medium, 10% FBS, 2 mM L-glutamine, and antibiotics. GL261 murine glioblastoma cells (a gift from Dr. David Zagzag, New York University, New York) were cultured in DMEM supplemented with 10% FBS, 2 mM L-glutamine, 1% non-essential amino acids, and antibiotics.

Binding Assays

$VEGF_{165}$ was labeled with $Na^{125}I$ using IODO-GEN (Pierce) as coupling agent according to the manufacturer's instructions. BAE, CHO-VEGFR2, and CHO-VEGFR1 cells were seeded at 2.5×10^5 density in gelatin-coated 6-well plates and cultured in complete medium for 2 days. Cells were washed twice with ice-cold PBS and incubated with 10 ng/ml ^{125}I-VEGF and peptides at indicated concentrations in binding medium (DMEM; 20 mM Hepes, pH 7.4; 0.15% gelatin) on a shaker at 4 °C. After 2 h, cells were washed 3 times with PBS and solubilized by the addition of 2% Triton, 10% glycerol, and 1 mg/ml bovine serum albumin prior to γ-counting. Each condition was tested in duplicate and repeated at least two times. Data are expressed as percentage of total radioactivity.

Proliferation Assays

BCE and BAE cells were seeded in 24-well culture plates overnight in 10% newborn calf serum at 7500 cells per well. Medium was changed to 1% newborn calf serum, 10 ng/ml growth factor, and peptides at indicated concentrations were added to duplicate wells. After 48 h, medium was changed, and stimulation with growth factor and peptide treatment were repeated. One day later, cells were counted on a Coulter counter. Balb3T3 were seeded at a density of 10,000 cells/well in complete medium. Medium was changed to 0.5% fetal calf serum and 20 ng/ml human recombinant PDGF-BB (Sigma), and peptides at indicated concentrations were added to duplicate wells. Cells were counted 2 days later. U87 and GL261 cells were seeded at 10,000 cells/well in 1% FBS, treated with peptides at the same concentrations as ECs, and counted 72 h later. Each condition was tested in duplicate and repeated at least two times.

ERK-1 (p44)/ERK-2 (p42) Phosphorylation Assay

BAE cells were plated in 35-mm plates. Subconfluent cultures were serum-deprived for 24 h. Peptides were then added for 6 min in the presence of 10 ng/ml $VEGF_{165}$. Cells were scraped off the dish and lysed for 10 min on ice in Nonidet P-40/SDS lysis buffer (50 mM Hepes, pH 7.4; 75 mM NaCl; 1 mM EDTA; 1% Nonidet P-40; 0.1% SDS) containing a mixture of protease inhibitors. The insoluble material was removed by centrifugation for 20 min at $12,000 \times g$ at 4 °C. The cleared supernatant was stored at −80 °C. Protein concentration was measured by using the Bradford method (Bio-Rad). The cytoplasmic extracts were resolved by SDS-PAGE on 12% gels under reducing conditions and electrotransferred onto a nitrocellulose membrane. The blocked membranes were then incubated with primary antibodies (phospho-specific mitogen-activated protein kinase p42/p44 or mitogen-activated protein kinase

[2] S. Shinkaruk, L. Zilberberg, X. Canron, C. Chauseau, M. Bayle, B. Desbas, A. Bikfalvi, and G. Deleris, manuscript in preparation.

p42/p44 were obtained from New England Biolabs, Ozyme, France), washed, and incubated with secondary horseradish peroxidase-conjugated mouse or rabbit antibodies (Dako SA, Trappes, France). Detection of antibodies was performed using the ECL*plus* Western blot detection system (Amersham Biosciences). Each condition was tested at least two times.

Migration Assay

Migration test with BAE cells was performed using a method described earlier (39). In brief, ECs were seeded in 350-mm culture plates and were allowed to grow to confluence. Complete medium was replaced with serum-free DMEM, and incubation was continued overnight. One linear scar was drawn in the monolayer and divided into seven equal fields. A set of digital photos was taken of each scar, and the denuded area was marked using digital image analysis software (Lucia G, www.lim.cz). The dishes were washed and incubated with fresh serum-free medium containing 0.1% bovine serum albumin, 10 ng/ml $VEGF_{165}$, and peptides at indicated concentrations. After 16 h, cells were fixed in 1% glutaraldehyde and counterstained (Giemsa), and a second set of photos was taken. Photos were superposed, and endothelial cells having migrated across the line drawn at the border of the scar in the first photo set were counted. Each condition was tested in two independent experiments. Means for all fields of each group were calculated; data are expressed in percentage of the mean number of migrated cells over $VEGF_{165}$-induced cell migration.

CAM Assay

Fertilized chicken eggs (*Gallus gallus*) (E.A.R.L. Morizeau, Dangers, France) were incubated at 37 °C and 80% humidified atmosphere. On day 4 of development, a window was made in the eggshell and sealed with Durapore® tape. On day 13, plastic rings (made from Nunc Thermanox® coverslips) were put on the CAM. 3 μg of $VEGF_{165}$ was premixed with 50 μg of peptides or with the equivalent volume of sterile water alone and deposed in the center of the plastic ring as described previously (21). Treatment was repeated the following day. On day 17, the CAMs were fixed *in vivo* with 4% paraformaldehyde for 30 min at room temperature, and the area containing the ring was cut out for further analysis. Photos of each CAM were taken under a stereomicroscope (Nikon SMZ800) using a digital camera (Nikon Coolpix 950). Two observers scored the angiogenic response from 0 to 3 (0 = none, 1 = medium, 2 = medium/high, and 3 = high). The angiogenic score was indicated as the mean number from the two observers. Statistical analysis was carried out using Student's two-tailed *t* test. For confocal studies, 6 CAM samples for each condition were processed. Each sample was washed by incubation with 0.1% Triton in PBS. Fluorescein-*Sambucus nigra* lectin (M0928 Vector Laboratories) at 40 μg/ml was added, and incubation was performed in 0.1% Triton/PBS for half an hour at room temperature. Samples were washed 3 times with 0.1% Triton/PBS, 3 times with PBS, and rinsed 3 times with water. The samples were finally mounted and embedded with Antifading Prolong (Molecular Probes, Eugene, OR) and viewed by confocal fluorescent microscopy at ×600 magnification equipped with an anti-bleed through control system based on sequential capture of the green signal (Nikon, PCM2000).

Animal Experiments

Short-term Experiments—Groups of 10 6-week-old nude mice (Charles River Italia, Italy) were implanted intracranially with 50,000 U87 glioma cells using an open window technique. For the syngeneic model, groups of 10 6-week-old BALB/c mice (Charles River Italia) were implanted intracranially with 50,000 GL261 glioma cells using the same technique.

In a first group of experiments, 12 days after tumor cell injection, groups of 10 nude or BALB/c mice each were treated intraperitoneally with 2 mg/kg/day of cyclo-VEGI or saline in a single shot. Treatment was continued for 28 days. Afterward, animals were sacrificed, and their brains were removed, embedded in OCT, and stored at −70 °C.

In a second group of experiments, 12 days after tumor cell injection, two groups of 10 nude mice each were implanted subcutaneously with 2004 Alzet osmotic minipumps. The pumps used in these experiments afford a constant period of work of 28 days. In the first group, the pump reservoir was filled with 0.45 mg (total amount) of the cyclo-VEGI, which corresponds to 0.45 mg/kg/day. The second group of 10 animals was implanted with pumps containing PBS, and a third additional group did not receive any pumps. The last two groups served as the controls for the experiment. Animals were sacrificed when signs of any distress were evident and after 29 days from implantation of the pumps. Then the brains were removed, embedded in OCT, and stored at −70 °C.

Long-term Experiments—For the long term experiments, groups of 10 nude mice each were implanted intracranially with 50,000 U87 glioblastoma cells using the same procedure described previously. Twelve days after tumor cell injection, a first group of animals was implanted subcutaneously with Alzet minipumps, and the reservoir was filled with 0.45 mg (total amount) of cyclo-VEGI (0.45 mg/kg/day). A second group of nude mice received subcutaneous minipumps containing saline and served as a control. Twenty-eight days later, the pump was changed with a new one containing the same amount of the inhibitor, in order to afford a 58-day period of treatment. Animals were carefully monitored for the occurrence of any side effects and immediately sacrificed at the occurrence of any neurological deficits. Seventy days after tumor cell implantation, all the remaining animals were sacrificed. All animal experiments were repeated at least two times.

All brains were fixed in 5% paraformaldehyde in PBS for 24 h at 4 °C, dehydrated in 30% sucrose in PBS for 24 h at 4 °C, embedded in OCT, and stored at −70 °C. The brains were then sectioned, and a portion of them submitted to routine histological examination with hematoxylin and eosin staining. Tumor volume was calculated and expressed as a mean ± S.E. Tumor volume was estimated using the formula for ellipsoid ($\text{width}^2 \times \text{length}$)/2. The remaining slides were used for the immunohistochemistry analysis as described below. Kaplan-Meyer survival curves were statistically analyzed using repeated measures analysis of variance.

Immunohistochemistry

Immunohistochemistry was performed on 5-μm sections. Immunohistochemistry on 5-μm sections was carried using the Vectastain Elite kit (Vector Laboratories). Primary antibodies include anti-CD31 (1:100 dilution, BD Biosciences) and anti-Ki-67 (1:100 dilution, Dako). Detection was carried out using DAB chromogen. Sections were counterstained with hematoxylin. Negative control slides were obtained by omitting the primary antibody. Ki-67 staining was quantified by counting the number of positively stained cells of 100 nuclei in 20 randomly chosen fields (40, 41). Microvessel count and density were scored as reported previously (40, 41). Apoptotic cells were detected with ApopTag™ plus kit (Genenco International, New York) with 1% methyl green as a counterstain. Apoptosis and proliferative indices were quantified by determining the percentage of positively stained cells for all nuclei in 20 randomly chosen fields per section at ×200 magnification (40).

RESULTS

Secondary and Three-dimensional Structure of Cyclo-VEGI

Secondary Structure—Standard NMR methodology was used to obtain sequence-specific assignments of proton resonances in water and in TFE/water mixtures at two different ratios, 15:85 or 30:70 (v/v). TOCSY spectra were used to identify spin systems, and NOESY spectra were used to obtain inter residue connectivities (42). The ^{13}C resonances of C^{α} carbons were assigned from ^{13}C-^{1}H HSQC spectra. Weak additional resonances could be observed in the NMR spectra recorded in water and also in TFE/water mixtures, albeit to a lesser extent. In the absence of chemical heterogeneity, a likely explanation of the observed chemical shift heterogeneity would be *cis-trans* isomerism of peptide bonds preceding proline. The major form corresponds to a *trans* conformation of the peptide bonds preceding the two Pro residues, as evidenced by the observation of strong $\alpha\delta$ (i − 1,i) sequential NOEs. The proportion of minor forms was too weak to give rise to NOE cross-peaks. However, the presence of alternative spin systems of Gln/Glu, Phe, His, and Lys in TOCSY spectra, *i.e.* amino acids around Pro residues, suggests that both D-Phe^1–Pro^2 and Lys^8–Pro^9 peptide bonds are likely to isomerize. The lower proportion of minor species in mixtures of TFE/water indicates that the stabilization of folded structures (see below) decreases the amount of *cis* isomers, as observed for cyclic gramicidin S.

The chemical shift deviations (CSDs) of H^{α} and C^{α} resonances, calculated as the difference between observed chemical

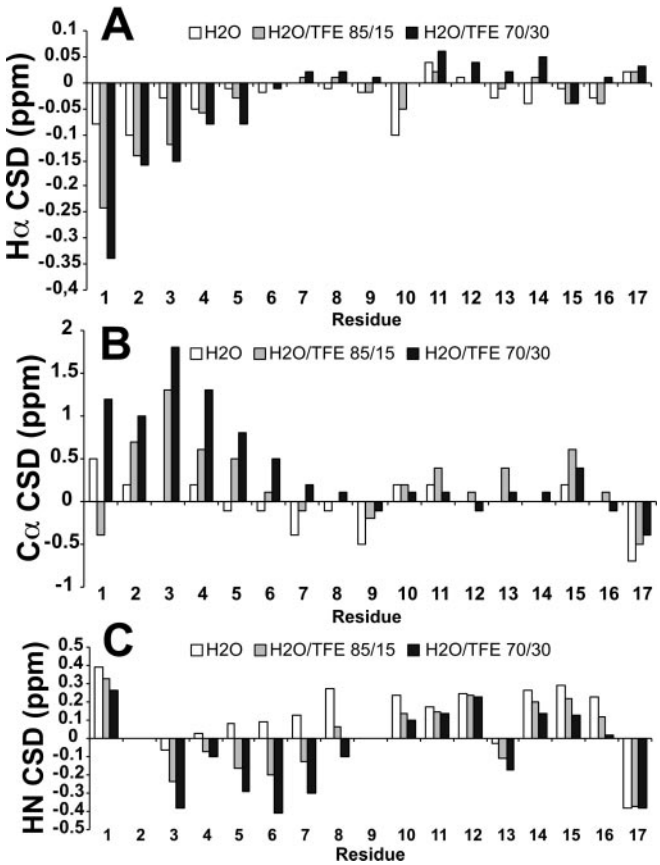

FIG. 1. **Hα (*A*), Cα (*B*), and HN (*C*) CSDs of cyclo-VEGI peptide in water and TFE/water mixtures.**

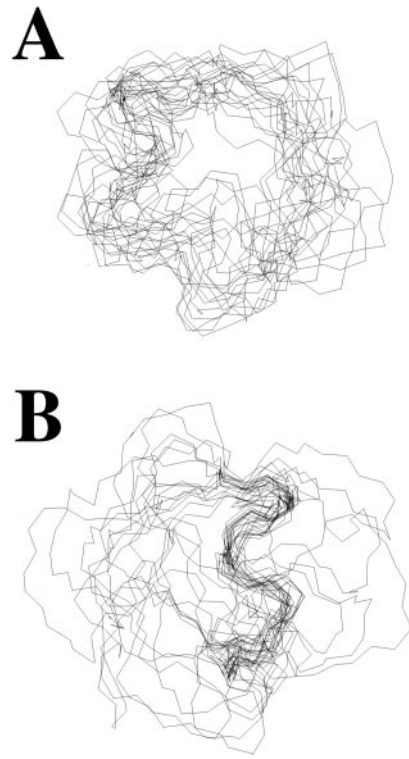

FIG. 2. **Backbone superimposition of the best 20 structures calculated in 30% TFE.** *A*, superimposition of residues 1–17. *B*, superimposition of residues 1–8, showing the helical domain.

shifts and corresponding random coil values, carry information about the secondary structure (43). A stretch of residues exhibiting upfield shifts of H^{α} protons and downfield shifts of C^{α} carbons is characteristic of a helix, whereas the observation of downfield shifts of H^{α} and upfield shifts of C^{α} indicates the presence of β-sheet structures. Fig. 1 shows the H^{α} and C^{α} CSDs in water and in TFE/water mixtures. The peptide in water displays very weak CSDs along its whole sequence, indicating that it is largely unstructured in aqueous solution. The addition of TFE (from 15 to 30%) progressively induces an upfield shift of H^{α} and a downfield shift of C^{α} resonances for residues 1–6, supporting the formation of a helical structure. Because the corresponding H^{α} CSDs are slightly negative in water, this suggests that the 1–6 segment has a small helical propensity in water and that helical conformations explored in this region are stabilized by the addition of TFE. Strong upfield shifts of amide protons chemical shifts are also induced by the addition of TFE for residues 3–8. Interestingly, these variations are opposite to those observed for cyclic gramicidin S under the same conditions and are correlated to the formation of a β-sheet structure. Furthermore, residues 3–8 exhibit weak temperature gradients of their amide proton chemical shifts ($\Delta\delta_{NH}/\Delta T$). Altogether, these chemical shift data are consistent with the formation of a helical structure in segment 1–8. No significant CSD variations could be observed in the other parts of the sequence, suggesting that the peptide remains unstructured, apart from the 1–8 region.

Three-dimensional Structure—The cyclic peptide shows few NOEs in water, besides intraresidual and sequential connectivities. In contrast, the peptide in 30% TFE exhibits NOEs characteristic of helical structure in segment 1–8, including strong dNN ($i,i+1$) and medium dαN ($i,i+1$) sequential connectivities, together with several dαN ($i,i+2$), dαN ($i,i+3$), and dαN ($i,i+4$) medium range connectivities. The structure of the cyclic peptide in 30% TFE was calculated by restrained molecular dynamics, using a set of 17 intraresidual, 63 sequential, and 20 medium range distance restraints. The best 20 calculated structures are shown in Fig. 2. They have low energies and few distance violations, indicating that they are in good agreement with NMR experimental restraints. The overall structure of the cyclic peptide is poorly defined, as evidenced by the large root mean square deviation of backbone atoms (3.4 Å). However, the superimposition of structures using backbone atoms of residues 1–8 or 1–6 shows that the backbone is better defined in this region, with corresponding root mean square deviations of 1.6 and 1.1 Å, respectively. Segment 1–8 adopts a helical conformation. Unexpectedly, residues D-Phe^1–Pro^2 do not form a type II′ β-turn but are rather part of the helical 1–8 segment, as shown by medium range correlations between D-Phe^1–Ile^4 and Pro^2–Met^5. Similarly, residues Pro^9–His^{10} do not form a stable β-turn. The conformations of other residues are not well defined but are not completely random coil due to the cyclic topological constraint.

Inhibition of VEGF Binding to Its Receptors

We first looked at the ability of cyclo-VEGI to interfere with binding of ^{125}I-labeled $VEGF_{165}$ to Chinese hamster ovary (CHO) cells expressing VEGFR2. Cyclo-VEGI inhibited ^{125}I-labeled $VEGF_{165}$ binding to VEGFR2 in a dose-dependent manner (Fig. 3*A*) with a half-maximal inhibition (IC_{50}) of 1.3 μM. The linear control peptide P14 with the same amino acid sequence as cyclo-VEGI did not compete for receptor binding even at the highest concentration tested (Fig. 3*A*). To investigate whether cyclo-VEGI inhibits binding of $VEGF_{165}$ to VEGFR2 specifically, we tested the effect of cyclo-VEGI on the binding of ^{125}I-labeled $VEGF_{165}$ to CHO cells expressing VEGFR1. Interestingly cyclo-VEGI also inhibited binding of VEGF to VEGFR1 (IC_{50} value of 0.7 μM, Fig. 3*B*). We next evaluated its effect on ^{125}I-labeled $VEGF_{165}$ binding to high affinity VEGF receptors

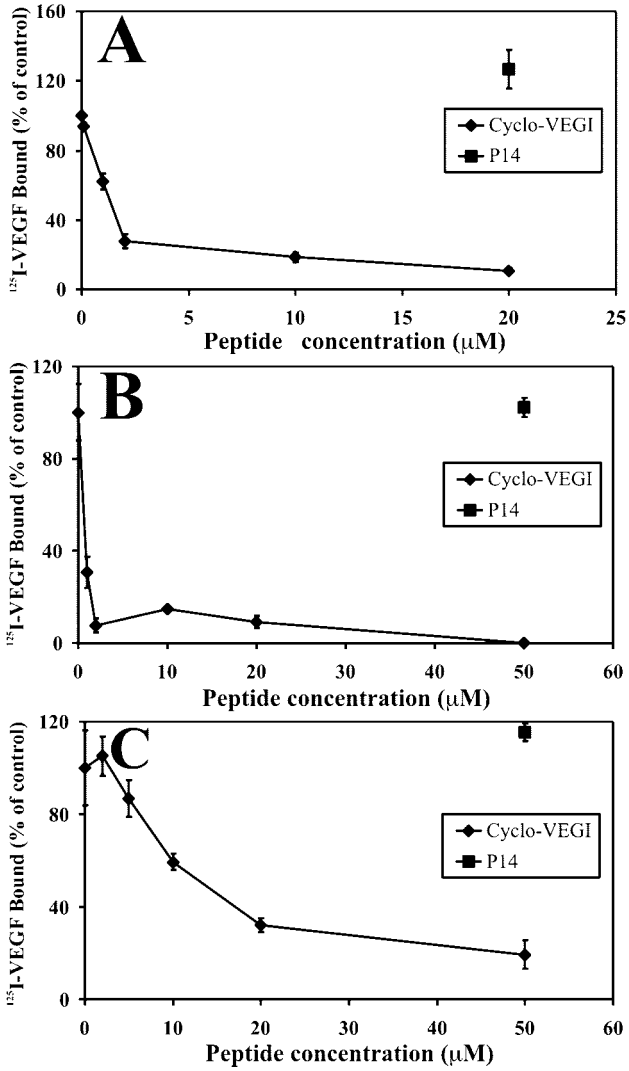

FIG. 3. **Inhibition of ^{125}I-VEGF$_{165}$ binding to CHO-VEGFR2 (*A*), CHO-VEGFR1 (*B*), and BAE (*C*) cells by cyclo-VEGI.** CHO-VEGFR2, CHO-VEGFR1, and BAE cells were incubated with 10 ng/ml ^{125}I-VEGF$_{165}$ and peptides at indicated concentrations. Cyclo-VEGI inhibited VEGF$_{165}$ binding in a dose-dependent manner, whereas the control peptide P14 did not, even at 100 μM on CHO-VEGFR2 cells (*A*), or 50 μM on CHO-VEGFR1 (*B*), and BAE (*C*) cells. The half-maximal inhibition (IC$_{50}$) values were 1.3, 0.7, and 12 μM for CHO-VEGFR2, CHO-VEGFR1, and BAE cells, respectively. Data represent means ± S.D. of duplicate experiments. The figure depicts a representative experiment from two independent experiments.

in BAE cells. As shown in Fig. 3*C*, cyclo-VEGI effectively inhibits the binding of ^{125}I-labeled VEGF$_{165}$ to high affinity receptors with an IC$_{50}$ of 12 μM. Linear control P14 at the highest concentration tested (50 μM) had no effect (Fig. 3*C*).

Inhibition of the Proliferation of Endothelial Cells but Not of Glioma Cells

We next investigated whether cyclo-VEGI inhibits VEGF-induced proliferation of BAE cells. When BAE cells were stimulated by 10 ng/ml of VEGF$_{165}$, cyclo-VEGI showed a dose-dependent inhibitory effect with an IC$_{50}$ of 5.8 μM, whereas the linear control P14 had no effect at the highest concentration tested (100 μM) (Fig. 4*A*).

VEGF is a member of the cystine-knot family of growth factors, with the highest sequence identity and structural similarity to PDGF-BB (44, 45). Moreover, endothelial cell proliferation is induced by FGF-2 (46). Thus, to investigate whether the effect of cyclo-VEGI on endothelial cells proliferation was

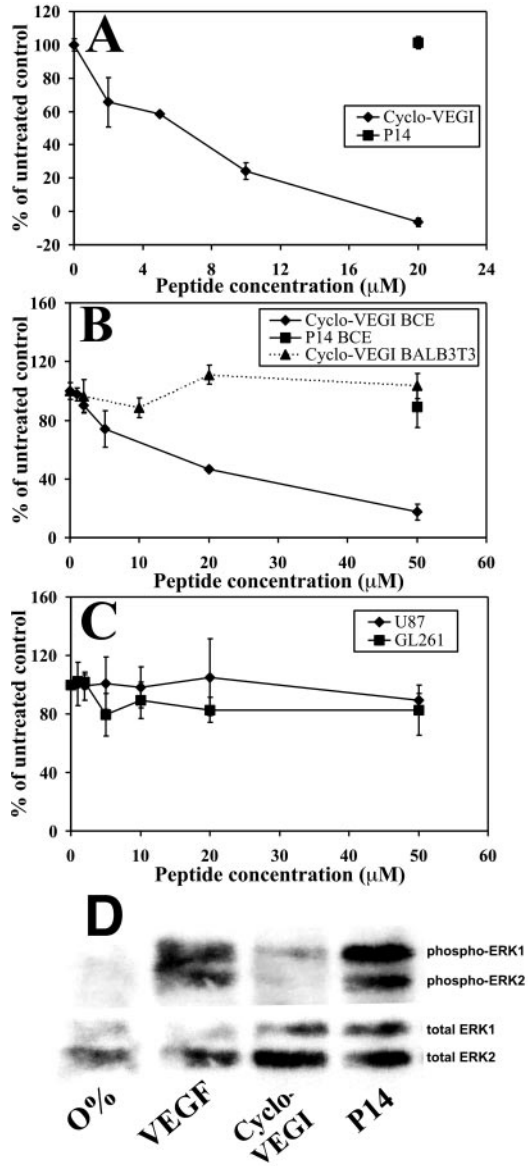

FIG. 4. **Effect of cyclo-VEGI on cell proliferation.** Proliferation was stimulated with 10 ng/ml VEGF$_{165}$ using BAE cells (*A*), 10 ng/ml FGF-2 using BCE cells (*B*), and 20 ng/ml PDGF-BB using Balb3T3 cells (*B*) and 1% serum using U87 and GL261 cells (*C*). *A*, cyclo-VEGI inhibited BAE cell proliferation in a concentration-dependent manner (IC$_{50}$ of 5.8 μM). 100% inhibition of proliferation was achieved with 20 μM cyclo-VEGI. The linear control P14 did not show any effect. *B*, cyclo-VEGI inhibited FGF-2-induced proliferation of BCE cells in a dose-dependent manner with an IC$_{50}$ of 18 μM. Peptide P14 had no effect. Cyclo-VEGI did not show any effect at all concentrations tested on PDGF-BB-induced Balb3T3. *C*, cyclo-VEGI did not show any effect at all concentrations tested on U87 and GL261 cells proliferation. Dose dependence experiments were performed in duplicates in two independent experiments; data of one experiment are shown. *D*, inhibition of VEGF-stimulated MAP kinase phosphorylation. Serum-deprived bovine aortic endothelial cells (*1st lane*) were stimulated with 10 ng/ml VEGF$_{165}$ (*2nd lane*) in the presence of 20 μM cyclo-VEGI (*3rd lane*), or 20 μM of linear control P14 (*4th lane*). Cell lysate blot was probed with phosphospecific ERK1 and ERK2 antibodies, and the total amount of MAPs protein loading was assessed by probing with MAP antibodies. Blots depict a representative experiment from two independent experiments.

specific for VEGF$_{165}$, we tested the activity of cyclo-VEGI on PDGF- or FGF-induced cell proliferation. When Balb3T3 cells were stimulated with 20 ng/ml PDGF-BB, cyclo-VEGI did not show any effect even at the highest concentration tested (50 μM) (Fig. 4*B*). Surprisingly, cyclo-VEGI decreased FGF-induced BCE proliferation, however three times less potently (IC$_{50}$ of 18

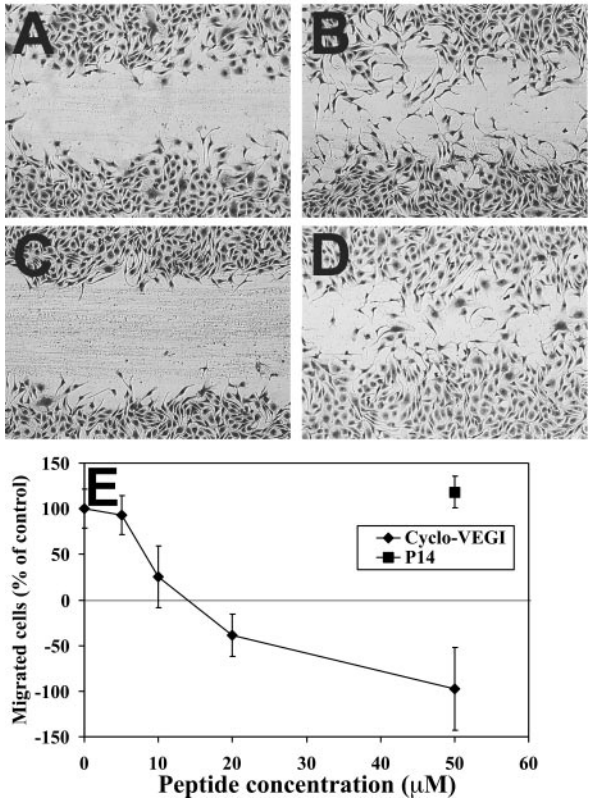

FIG. 5. **Migration of BAE cells in the presence of $VEGF_{165}$ and different concentrations of cyclo-VEGI.** BAE migration was stimulated with 10 ng/ml $VEGF_{165}$. *A*, after 16 h in serum-free medium, some random cell migration occurred. *B*, $VEGF_{165}$ induces cell migration into the denuded area of the scar. At 50 μM, linear control P14 (*D*) had no effects, whereas cyclo-VEGI (*C*) completely abolished $VEGF_{165}$-induced endothelial cell migration. *E*, cyclo-VEGI reduces migration of the endothelial cells in a dose-dependent manner. *Horizontal line* at 0 indicates conditions where 100% inhibition of VEGF-induced migration is reached. Data are expressed in percentage of the mean number of migrated cells of seven fields over $VEGF_{165}$-induced cells migration. Dose dependence experiments were performed in two independent experiments; data of one experiment are shown.

μM in comparison to 5.8 μM for VEGF-induced endothelial cell proliferation) (Fig. 4*B*). Proliferation of two glioma cell lines, human U87 and mouse GL261 cells, was not inhibited by cyclo-VEGI peptides at all the concentrations tested (Fig. 4*C*).

Inhibition of VEG_{165} Signal Transduction

We next investigated the effect of cyclo-VEGI on ERK1 and ERK2 phosphorylation. As expected, activation of VEGFR2 with 10 ng/ml $VEGF_{165}$ in BAE cells induced a strong phosphorylation of ERK1 and ERK2 (Fig. 4*D*, *2nd lane*). Cyclo-VEGI, at 20 μM, completely suppressed VEGF-induced ERK1 and ERK2 phosphorylation (Fig. 4*D*, *3rd lane*). The linear control P14 did not show any inhibitory effect on $VEGF_{165}$-induced phosphorylation of ERK1 and ERK2 (Fig. 4*D*, *4th lane*). Similar results were also observed on human umbilical vein endothelial cells stimulated with 10 ng/ml of $VEGF_{165}$ (data not shown).

Inhibition of Endothelial Cell Migration

We then investigated whether endothelial cell motility, an important pre-requisite for angiogenesis, was affected by cyclo-VEGI. The wounding assay was used to determine the effect of cyclo-VEGI on VEGF-induced bovine aortic endothelial cells migration *in vitro*. In the absence of VEGF, some random background migration occurred (Fig. 5*A*). When stimulated with $VEGF_{165}$, an increased number of BAE cells migrated into the denuded scar area (Fig. 5*B*). Migration was not affected when the linear control peptide (P14) was added (Fig. 5, *D* and *E*). On the contrary, cyclo-VEGI inhibited VEGF-induced migration of endothelial cells in a dose-dependent manner with an IC_{50} of 8.2 μM (Fig. 5, *C* and *E*). Inhibition of migration of the endothelial cells below base-line levels was also observed (Fig. 5*E*).

Inhibition of VEGF-induced Angiogenesis on the CAM

Peptides were tested in the differentiated CAM assay, where capillary angiogenesis is induced by $VEGF_{165}$ (21). For this experiment, a plastic ring is filled in the center with 3 μg of $VEGF_{165}$ alone or with $VEGF_{165}$ plus either the vehicle alone (water), 50 μg of cyclo-VEGI, or 50 μg of the control peptide P14. Recombinant human $VEGF_{165}$ alone induced significant angiogenesis (Fig. 6, *B* and *I*). Some stimulation is also present around the site of application because of diffusion of the growth factor. Vehicle alone (water) in the plastic ring had no effect (Fig. 6, *A* and *I*). When premixed with $VEGF_{165}$ and deposed on the CAM, a clear anti-angiogenic effect of cyclo-VEGI was visible inside the ring (Fig. 6, *C* and *I*). The linear control P14 did not inhibit VEGF-induced capillary growth in the CAM (Fig. 6, *D* and *I*). 50 μg of cyclo-VEGI applied alone on the CAM without $VEGF_{165}$ did not show any effect or toxicity (data not shown).

The capillary structure in the stroma was also examined by immunohistology and confocal microscopy. Vessels were visualized by staining endothelial cells with fluorescein isothiocyanate (FITC) conjugated to *S. nigra* lectin. This lectin interacts preferentially to sialic acid attached to terminal galactose by α-2,6-link and was shown to bind endothelial cells in the CAM. The extensive characterization of the CAM vasculature using this method will be described elsewhere.[3] $VEGF_{165}$ induced a strong increase in vessel density, a reduction of the intercapillary space, and structures suggestive of ongoing fusion events between small vessels (Fig. 6*F*). These chaotic vascular structures were not present when cyclo-VEGI was added together with $VEGF_{165}$ in the plastic ring (Fig. 6*G*). However, some neovessels remained, as evidenced by a slightly higher microvessel density compared with control CAM treated with water alone (Fig. 6, *G* and *E*). CAMs treated with control peptide P14 with $VEGF_{165}$ had a similar morphology than CAMs treated with $VEGF_{165}$ alone (Fig. 6*H*).

Inhibition of Glioma Growth in Vivo

The ability of cyclo-VEGI to reduce glioma growth *in vivo* was initially investigated by short term studies. In these experiments, nude mice implanted intracranially with human glioblastoma cells were treated intraperitoneally with 2 mg/kg/day of cyclo-VEGI. Treatment was started 12 days after tumor cell implantation in order to treat well established tumors. Twenty eight days later, the treatment was stopped, and the animals were sacrificed. Histological analysis of the brains from treated and untreated animals showed that treatment with cyclo-VEGI was associated with a 70% reduction of U87 tumor growth (Fig. 7*A*, *lower panel*). A similar significant inhibition (78%) was observed in immunocompetent BALB/c mice implanted with GL261 murine glioblastoma cells (Fig. 7*A*, *top panel*).

In a second set of experiments we investigated the ability of cyclo-VEGI to reduce U87 glioma growth when administered continuously and systemically by subcutaneous minipumps in nude mice. In these experiments, the pump reservoirs were filled with 0.45 mg/kg/day of the inhibitor. Analysis of tumor

[3] M. Hagedorn, M. Balke, A. Schmidt, W. Bloch, H. Kurz, S. Javerzat, B. Rousseau, J. Wieting, and A. Bikfalvi, submitted for publication.

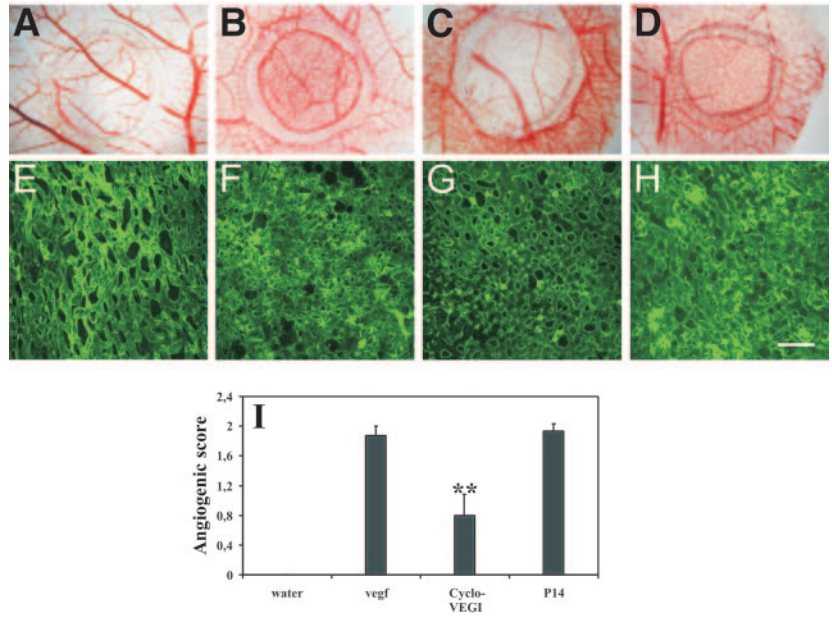

FIG. 6. **Anti-angiogenic activity of cyclo-VEGI in the chick CAM assay.** *A–D*, images of representative CAMs for each condition are shown (*A*, water, $n = 12$. *B*, $VEGF_{165}$, $n = 27$. *C*, cyclo-VEGI, $n = 40$. *D*, P14, $n = 22$). *E–H*, confocal observation of representative CAMs for each condition are shown (*white bar* equals 50 μm for all photos). *I*, angiogenic score was determined by scoring from 0 to 3 the appearance of the brush-like capillary formation by two independent observers. Sterile water alone did not interfere with CAM vasculature (*A*, *E*, and *I*). $VEGF_{165}$ induced a strong brush-like capillary formation (*B*, *F*, and *I*). Control peptide P14 was not able to impair growth of new capillaries (*D*, *H*, and *I*). Neoangiogenesis was significantly reduced nearly to control level in the CAMs that received $VEGF_{165}$ plus 50 μg of cyclo-VEGI (*C*, *G*, and *I*). Statistical analysis (Student's two-tailed *t* test) proved the difference between $VEGF_{165}$ and cyclo-VEGI to be significant (**, $p < 0.001$, *I*).

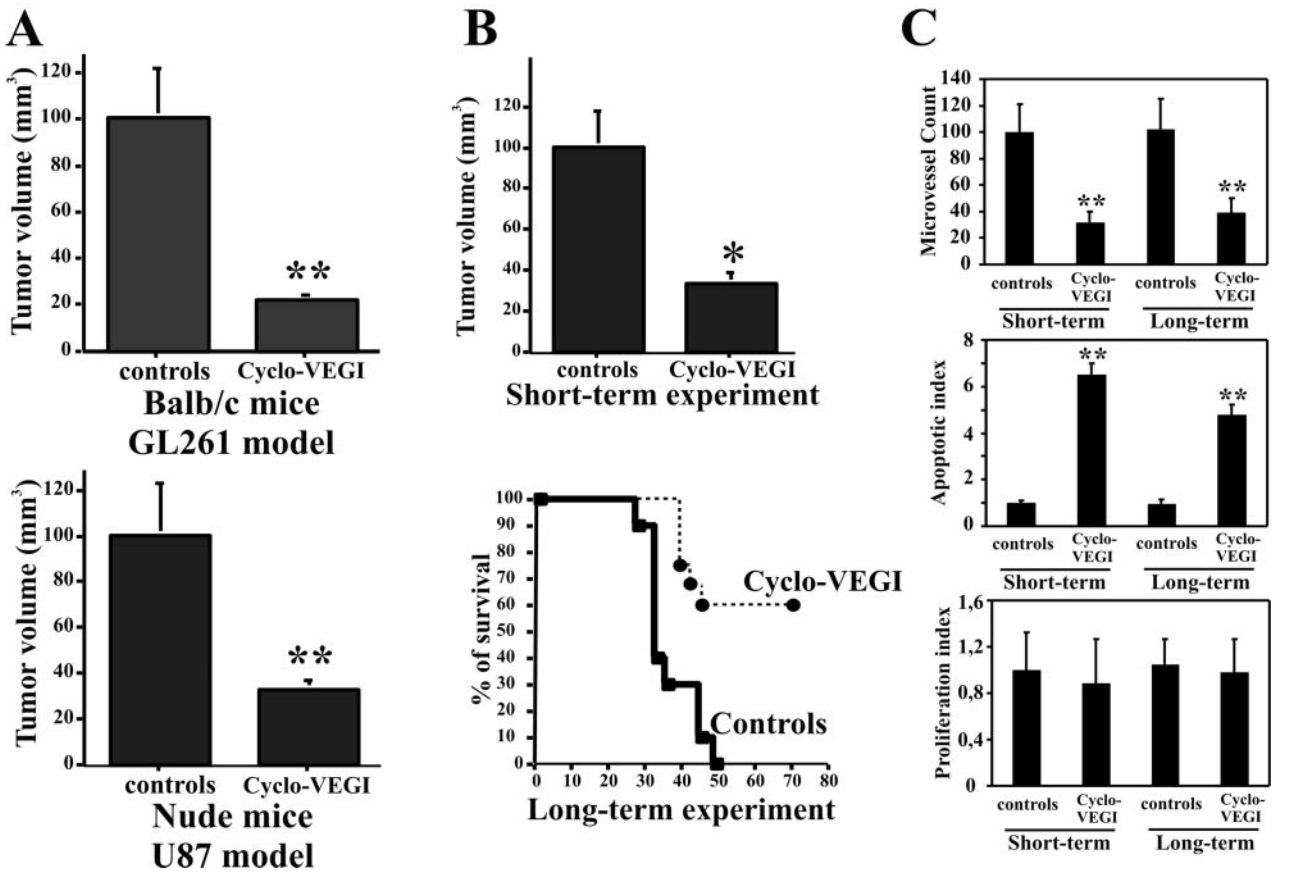

FIG. 7. **Cyclo-VEGI induces regression of gliomas in nude and syngeneic mice.** *A*, cyclo-VEGI reduced significantly the growth of human U87 glioma xenografts in nude mice (*lower panel*, **, $p < 0.001$) and GL261 glioma in immunocompetent BALB/c mice (*top panel*, **, $p < 0.001$). Mice were treated intraperitoneally with 2 mg/kg/day cyclo-VEGI. *B*, U87 glioma bearing-mice were treated with cyclo-VEGI administrated continuously and systemically by subcutaneous minipumps, and the reservoir was filled with 0.45 mg/kg/day cyclo-VEGI. In short-term experiments, the tumors of the mice treated with cyclo-VEGI were significantly smaller than those of the control mice (*top panel*, 72% inhibition and *, $p < 0.05$). In long-term studies, tumor-bearing mice treated with cyclo-VEGI survived significantly longer than those in the control group (75 and 32 days of 50% survival respectively, *lower panel*). *C*, CD31 staining of tumor samples revealed a decrease in the numbers of vessels in the cyclo-VEGI-treated group compared with PBS-treated tumors (*top panel* and **, $p < 0.001$). Increased apoptotic indices in samples from the cyclo-VEGI-treated tumors were observed compared with PBS-treated mice (*middle panel* and **, $p < 0,001$). Ki-67 staining revealed that cyclo-VEGI has no effect on tumor cell proliferation compared with PBS-treated tumors (*lower panel*).

volumes showed that continuous systemic administration of peptide cyclo-VEGI resulted in a 72% inhibition of intracranial glioma growth (Fig. 7*B*, *top panel*).

The same experimental design was used to perform long-term experiments. In these studies, the pump reservoirs were changed with a new one containing the same amount of the

inhibitor 28 days after implantation. Animals belonging to the control group showed a 50% survival of 32 days. Animals treated with cyclo-VEGI had a 50% survival of 75 days. No side effects were registered during the entire duration of the treatment (Fig. 7*B*, *lower panel*).

Histological Analysis

We next performed histological analysis of U87 glioma sections from the short-term and long-term experiments (using the subcutaneous minipumps). To quantify angiogenesis in these tumors, we stained endothelial cells for the expression of CD31. Treatment of U87 tumors with cyclo-VEGI reduced microvessel density by 68 and 62% when compared with PBS-treated controls for short-term and long-term experiments, respectively (Fig. 7*C*, *top panel*). A more detailed analysis revealed that, in control tumors, 55% capillary-like structures, 35% teleangiectatic or dilated vessels, and 10% glomeruloid structures were present. In cyclo-VEGI-treated tumors, 85% capillary structures, 15% teleangiectatic or dilated vessels, and no glomeruloid structures were observed. This indicates that vessels tends to be normalized by cyclo-VEGI treatment. Apoptotic indices quantified *in situ* by labeling fragmented DNA using the terminal deoxynucleotidyltransferase-mediated nick end labeling method were increased in tumors treated with cyclo-VEGI compared with PBS-treated controls (Fig. 7*C*, *middle panel*). An examination of proliferating cells within the tumor using Ki-67 nuclear antigen staining revealed no differences in the proliferating indices between PBS-treated controls and any cyclo-VEGI-treated groups (Fig. 7*C*, *lower panel*).

DISCUSSION

Structural and mutagenesis studies have shown that the residues within the amino acid sequence 79–93 of VEGF are involved in its interaction with VEGFR2 and that Arg^{82}, Lys^{84}, and His^{86} are key residues. The x-ray structure of VEGF-A revealed that this sequence is located within a β-sheet structure formed by two anti-parallel strands (β5 and β6) and connected by a type II β-turn (27–29, 47). We designed linear and cyclic peptides based on this sequence and tested them for inhibition of $VEGF_{165}$ binding to VEGFR2. It appears that a 17-amino acid cyclic peptide (CBO-P11), herein designated cyclo-VEGI, inhibits very efficiently the binding of VEGF to its receptor VEGFR2.[2] In this article, we undertook a series of systematic studies to determine the structural and biological properties of this peptide.

In aqueous solution, the cyclic peptide presents a weak propensity to adopt a helix structure in the 1–8 domain. The addition of TFE stabilizes helical conformations in this region, without any noticeable effect on the structure of the other parts of this peptide. TFE is known to strengthen intramolecular hydrogen bonds in peptides. The stabilization of the secondary structure by TFE has been observed for cyclic analogs of gramicidin S containing $4n + 2$ residues, but intramolecular hydrogen bonding occurs between two strands in this latter case, resulting in the stabilization of β-sheet structures (48). The property of this cyclic peptide to adopt helical conformations was largely unexpected because mostly β-sheet structures or random coil conformations have been observed for macrocyclic peptides (49).

Pro has two opposite roles as inducer of helical structure when located at the N terminus or helix breaker or bender when found in the middle of a helical domain. In this cyclic peptide, Pro^2 and Pro^9 have these two opposite effects. Indeed, Pro^2 induces the formation of helix, whereas Pro^9 breaks the 1–8 helical domain. The heterochiral D-Phe-Pro sequence is known to adopt either a type II′ β-turn or a γ-turn in small cyclic peptides. In this macrocyclic peptide, Pro^2 is not part of a type II′ β-turn and initiates helix formation. Thus, despite the presence of a motif known to stabilize a type II′ β-turn in β-hairpins, the peptide does not adopt a β-sheet structure. However, it is not in a random coil state, because region 1–8 of the peptide explores helical conformations. This topology could open new possibilities in the design of scaffolds for protein engineering, because further chemical modifications, such as C^{α} methylation, could be used to stabilize the α-helical domain. The residues Arg^{82}, Lys^{84}, and His^{86} localized in the β-hairpin 79–93 of VEGF are implicated in the binding to the VEGFR2 receptor. In this VEGF cyclic peptide, they are found at the end of the helical domain. Their side chains are not well defined, and it is likely that they retain enough conformational flexibility in the cyclic peptide to explore the orientation required for binding to the VEGF receptors and to prevent VEGF binding.

Although VEGFR1 binds VEGF with 50-fold higher affinity than VEGFR2, most of the VEGF angiogenic properties like mitogenicity and migration of endothelial cells are mediated by interaction with VEGFR2 (6, 50). Thus, our initial goal was to design peptides that specifically interfere with binding of VEGF to its receptor VEGFR2. Indeed, cyclo-VEGI did interfere with $VEGF_{165}$ binding on CHO-VEGFR2 in a dose-dependent manner. The linear control peptide P14 with the same amino acid sequence as cyclo-VEGI did not compete for receptor binding even at the highest concentration tested (Fig. 3*A*). This indicates that the inhibitory effect of cyclo-VEGI is structure-dependent. This result is in agreement with the results of other groups who showed that residues 82–90 in the loop between β-strands 5 and 6 of VEGF are critical for binding to and activation of VEGFR2 (51, 52). This loop is part of the cyclo-VEGI peptide we have designed. Surprisingly, our peptide also inhibited the binding of $VEGF_{165}$ to VEGFR1. One possible explanation for this finding might be that the receptor binding domain determinants of $VEGF_{165}$ for VEGFR1 and VEGFR2 share similar residues. Indeed, crystallographic studies of VEGF bound to the second Ig-like domain of VEGFR1 and mutagenesis analysis of the binding surface of VEGF for VEGFR2 revealed that some but not all residues in this loop domain are important for the binding to both receptors, VEGFR1 and VEGFR2 (27, 28).

Treatment of BAE cells with micromolar concentration of cyclo-VEGI strongly inhibited $VEGF_{165}$-induced cell proliferation. Although selectivity was observed for inhibition of VEGF-induced proliferation of endothelial cells in comparison to the structurally related growth factor PDGF-BB, cyclo-VEGI was also found to impair FGF-2-induced endothelial cell proliferation. Nevertheless, the activity of cyclo-VEGI appears to be severalfold lower toward FGF-2 than toward VEGF. This effect of cyclo-VEGI on FGF-2-induced proliferation was rather unexpected but may constitute an advantage for several reasons. First, it has been shown previously that FGF-2 can induce production of VEGF via an autocrine feedback loop and that both growth factors can synergize with respect to their ability to induce angiogenesis (53, 54). Second, this might prove beneficial *in vivo*, because tumor cells can produce both VEGF and FGF-2 and their inhibition has a synergistic effect in the impairment of tumor growth (55, 56). This is also illustrated by the observation that a modified peptide derived from platelet factor-4, which inhibits FGF-2 and $VEGF_{165}$-induced endothelial proliferation, had a strong inhibitory effect on human intracranial established glioma growth (21). The reasons for the effect of cyclo-VEGI on FGF-2 activity are not clearly understood. HSPGs are molecules found on the cell surface of almost all mammalian cells and have been shown to modulate the biological activity of growth factors (57). FGF-2 and $VEGF_{165}$ function in concert with cell surface-bound HSPGs to promote

binding to their specific receptors and to induce their biological responses (58). We cannot rule out the possibility for cyclo-VEGI to bind to the cell surface heparan sulfate proteoglycans (HSPGs) because of its basic residues, thus preventing the binding of $VEGF_{165}$ and FGF-2 to their receptors and subsequently inhibiting proliferation of endothelial cells. However, the linear control peptide P14, which has the same sequence as cyclo-VEGI, does not have any antagonist effect on FGF-2 or $VEGF_{165}$-induced proliferation even at the highest dose of 100 μM. This finding suggests that cyclo-VEGI inhibits FGF-2-induced endothelial cell proliferation by another mechanism, probably involving specific structural properties of this cyclic peptide. Preliminary experiments indicate that cyclo-VEGI also impairs FGF-2 binding to endothelial cells, although at higher cyclo-VEGI concentrations. Further studies are underway to solve this issue.

To substantiate further the antagonist activity of cyclo-VEGI, we tested its activity on VEGF-induced signaling and migration. MAP kinases play a central role in controlling growth signals from growth factor receptor tyrosine kinases such as VEGFR2 (59). In agreement with the effect of cyclo-VEGI on VEGF-induced endothelial cell proliferation, we also observed an inhibition of MAP kinase activation by cyclo-VEGI in endothelial cells upon VEGF stimulation. Migration of endothelial cells, an important pre-requisite for angiogenesis, was also affected by cyclo-VEGI in a dose-dependent manner. Cyclo-VEGI inhibited EC migration below 0% serum control levels which suggests that residual VEGF was still present in the media. This may be due to the presence of residual $VEGF_{165}$ attached to HSPGs on endothelial cells or of VEGF produced by endothelial cells themselves (60, 61).

We next tested effects of cyclo-VEGI for its ability to interfere with $VEGF_{165}$-induced angiogenesis on the differentiated day 13 CAM (62). The typical brush-like formation of capillaries in the stroma of the CAM induced by human recombinant $VEGF_{165}$ is strongly reduced by cyclo-VEGI peptides at 50 μg and not by linear control peptide P14. Cyclic peptide antagonists for $\alpha_V\beta_3$ integrin showed strong anti-angiogenic effects in the day 10 CAM at 300 μg. Angiogenesis was also induced by VEGF at lower doses than in our assay (1 *versus* 6 μg) (63). These comparisons indicate that cyclo-VEGI inhibits VEGF-induced angiogenesis *in vivo* in a very efficient way.

Gliomas constitute the most frequent class of primary brain tumors and are among the most malignant cancers, often resulting in the death of affected patients within months (64). In our model, established human intracranial glioma in nude mice decreased significantly by ~70% in size when treated with cyclo-VEGI in short and long term experiments. Moreover tumor-bearing mice treated with cyclo-VEGI lived significantly longer than those in the control group. Highly vascularized brain tumors such as gliomas produce high levels of VEGF in culture (56, 65). The decreased number of vessels for the cyclo-VEGI-treated tumors is consistent with a direct inhibition of VEGF signaling (as observed in our *in vitro* experiments) which in turn impairs tumor growth. This is also in agreement with an indirect (*i.e.* anti-angiogenic) antitumor effect rather than a direct antiproliferative effect on the tumor cells as evidenced by the absence of effect of cyclo-VEGI on the proliferation of tumor cells *in vitro* and *in vivo*. Histological analysis of cyclo-VEGI-treated gliomas showed characteristic findings observed in tumors treated with other potent anti-angiogenic compounds like endostatin and angiostatin. Although the proliferation index remained unchanged in tumor tissue irrespective of treatment, cyclo-VEGI decreased microvessel density which was accompanied by an increase in the apoptotic index as observed previously for other angiogenesis inhibitors (66, 67).

Taken together, these results indicate that cyclo-VEGI exhibits unique structural features and inhibits angiogenesis and tumor development *in vivo*. Furthermore, its inhibitor activity affects multiple angiogenesis pathways. Cyclo-VEGI is a promising candidate for the development of new cyclic angiogenesis inhibitor molecules useful for the treatment of cancer or other angiogenesis-related diseases.

Acknowledgments—We thank Dr. H. Prats for providing recombinant human FGF-2 and Dr. J. Plouët for providing CHOmVEGFR2, CHOmVEGFR1 cells, and baculovirus encoding human $VEGF_{165}$.

REFERENCES

1. Bikfalvi, A., and Bicknell, R. (2002) *Trends Pharmacol. Sci.* **23,** 576–582
2. Ferrara, N. (2002) *Nat. Rev. Cancer* **2,** 795–803
3. Javerzat, S., Auguste, P., and Bikfalvi, A. (2002) *Trends Mol. Med.* **8,** 483–489
4. Risau, W. (1997) *Nature* **386,** 671–674
5. Inoue, M., Hager, J. H., Ferrara, N., Gerber, H. P., and Hanahan, D. (2002) *Cancer Cell* **1,** 193–202
6. Neufeld, G., Cohen, T., Gengrinovitch, S., and Poltorak, Z. (1999) *FASEB J.* **13,** 9–22
7. de Vries, C., Escobedo, J. A., Ueno, H., Houck, K., Ferrara, N., and Williams, L. T. (1992) *Science* **255,** 989–991
8. Millauer, B., Wizigmann-Voos, S., Schnurch, H., Martinez, R., Moller, N. P., Risau, W., and Ullrich, A. (1993) *Cell* **72,** 835–846
9. Dvorak, H. F., Sioussat, T. M., Brown, L. F., Berse, B., Nagy, J. A., Sotrel, A., Manseau, E. J., Van de Water, L., and Senger, D. R. (1991) *J. Exp. Med.* **174,** 1275–1278
10. Relf, M., LeJeune, S., Scott, P. A., Fox, S., Smith, K., Leek, R., Moghaddam, A., Whitehouse, R., Bicknell, R., and Harris, A. L. (1997) *Cancer Res.* **57,** 963–969
11. Dirix, L. Y., Vermeulen, P. B., Pawinski, A., Prove, A., Benoy, I., De Pooter, C., Martin, M., and Van Oosterom, A. T. (1997) *Br. J. Cancer* **76,** 238–243
12. Gasparini, G., Toi, M., Gion, M., Verderio, P., Dittadi, R., Hanatani, M., Matsubara, I., Vinante, O., Bonoldi, E., Boracchi, P., Gatti, C., Suzuki, H., and Tominaga, T. (1997) *J. Natl. Cancer Inst.* **89,** 139–147 .
13. Rak, J., Yu, J. L., Kerbel, R. S., and Coomber, B. L. (2002) *Cancer Res.* **62,** 1931–1934
14. Kim, K. J., Li, B., Winer, J., Armanini, M., Gillett, N., Phillips, H. S., and Ferrara, N. (1993) *Nature* **362,** 841–844
15. Millauer, B., Shawver, L. K., Plate, K. H., Risau, W., and Ullrich, A. (1994) *Nature* **367,** 576–579
16. Robinson, G. S., Pierce, E. A., Rook, S. L., Foley, E., Webb, R., and Smith, L. E. (1996) *Proc. Natl. Acad. Sci. U. S. A.* **93,** 4851–4856
17. Skobe, M., Rockwell, P., Goldstein, N., Vosseler, S., and Fusenig, N. E. (1997) *Nat. Med.* **3,** 1222–1227
18. Wedge, S. R., Ogilvie, D. J., Dukes, M., Kendrew, J., Chester, R., Jackson, J. A., Boffey, S. J., Valentine, P. J., Curwen, J. O., Musgrove, H. L., Graham, G. A., Hughes, G. D., Thomas, A. P., Stokes, E. S., Curry, B., Richmond, G. H., Wadsworth, P. F., Bigley, A. L., and Hennequin, L. F. (2002) *Cancer Res.* **62,** 4645–4655
19. Ramakrishnan, S., Olson, T. A., Bautch, V. L., and Mohanraj, D. (1996) *Cancer Res.* **56,** 1324–1330
20. Siemeister, G., Schirner, M., Reusch, P., Barleon, B., Marme, D., and Martiny-Baron, G. (1998) *Proc. Natl. Acad. Sci. U. S. A.* **95,** 4625–4629
21. Hagedorn, M., Zilberberg, L., Wilting, J., Canron, X., Carrabba, G., Giussani, C., Pluderi, M., Bello, L., and Bikfalvi, A. (2002) *Cancer Res.* **62,** 6884–6890
22. Fairbrother, W. J., Christinger, H. W., Cochran, A. G., Fuh, G., Keenan, C. J., Quan, C., Shriver, S. K., Tom, J. Y., Wells, J. A., and Cunningham, B. C. (1998) *Biochemistry* **37,** 17754–17764
23. Binetruy-Tournaire, R., Demangel, C., Malavaud, B., Vassy, R., Rouyre, S., Kraemer, M., Plouet, J., Derbin, C., Perret, G., and Mazie, J. C. (2000) *EMBO J.* **19,** 1525–1533
24. Hetian, L., Ping, A., Shumei, S., Xiaoying, L., Luowen, H., Jian, W., Lin, M., Meisheng, L., Junshan, Y., and Chengchao, S. (2002) *J. Biol. Chem.* **277,** 43137–43142
25. Bae, D. G., Gho, Y. S., Yoon, W. H., and Chae, C. B. (2000) *J. Biol. Chem.* **275,** 13588–13596
26. Holash, J., Davis, S., Papadopoulos, N., Croll, S. D., Ho, L., Russell, M., Boland, P., Leidich, R., Hylton, D., Burova, E., Ioffe, E., Huang, T., Radziejewski, C., Bailey, K., Fandl, J. P., Daly, T., Wiegand, S. J., Yancopoulos, G. D., and Rudge, J. S. (2002) *Proc. Natl. Acad. Sci. U. S. A.* **99,** 11393–11398
27. Muller, Y. A., Li, B., Christinger, H. W., Wells, J. A., Cunningham, B. C., and de Vos, A. M. (1997) *Proc. Natl. Acad. Sci. U. S. A.* **94,** 7192–7197
28. Wiesmann, C., Fuh, G., Christinger, H. W., Eigenbrot, C., Wells, J. A., and de Vos, A. M. (1997) *Cell* **91,** 695–704
29. Keyt, B. A., Nguyen, H. V., Berleau, L. T., Duarte, C. M., Park, J., Chen, H., and Ferrara, N. (1996) *J. Biol. Chem.* **271,** 5638–5646
30. Piotto, M., Saudek, V., and Sklenar, V. (1992) *J. Biomol. NMR* **2,** 661–665
31. Bax, A., and Davis, D. G. (1985) *J. Magn. Reson.* **65,** 355–360
32. Kumar, A., Ernst, R. R., and Wuthrich, K. (1980) *Biochem. Biophys. Res. Commun.* **95,** 1–6
33. Schleucher, J., Schwendinger, M., Sattler, M., Schmidt, P., Schedletzky, O., Glaser, S. J., Sorensen, O. W., and Griesinger, C. (1994) *J. Biomol. NMR* **4,** 301–306
34. Wishart, D. S., Bigam, C. G., Holm, A., Hodges, R. S., and Sykes, B. D. (1995) *J. Biomol. NMR* **5,** 67–81
35. Wuthrich, K., Billeter, M., and Braun, W. (1983) *J. Mol. Biol.* **169,** 949–961
36. Weiner, S. J., Kollmann, P. A., Nguyen, D. T., and Case, D. A. (1986) *J. Com-*

put. Chem. **7,** 230–252
37. Cohen, T., Gitay-Goren, H., Neufeld, G., and Levi, B. Z. (1992) *Growth Factors* **7,** 131–138
38. Plouet, J., Schilling, J., and Gospodarowicz, D. (1989) *EMBO J.* **8,** 3801–3806
39. Hagedorn, M., Zilberberg, L., Lozano, R. M., Cuevas, P., Canron, X., Redondo-Horcajo, M., Gimenez-Gallego, G., and Bikfalvi, A. (2001) *FASEB J.* **15,** 550–552
40. Bello, L., Giussani, C., Carrabba, G., Pluderi, M., Lucini, V., Pannacci, M., Caronzolo, D., Tomei, G., Villani, R., Scaglione, F., Carroll, R. S., and Bikfalvi, A. (2002) *Clin. Cancer Res.* **8,** 3539–3548
41. Bello, L., Lucini, V., Carrabba, G., Giussani, C., Machluf, M., Pluderi, M., Nikas, D., Zhang, J., Tomei, G., Villani, R. M., Carroll, R. S., Bikfalvi, A., and Black, P. M. (2001) *Cancer Res.* **61,** 8730–8736
42. Wüthrich, K. (1986) *NMR of Proteins and Nucleic Acids*, John Wiley & Sons, Inc., New York
43. Wishart, D. S., Sykes, B. D., and Richards, F. M. (1991) *J. Mol. Biol.* **222,** 311–333
44. Oefner, C., D'Arcy, A., Winkler, F. K., Eggimann, B., and Hosang, M. (1992) *EMBO J.* **11,** 3921–3926
45. Muller, Y. A., Christinger, H. W., Keyt, B. A., and de Vos, A. M. (1997) *Structure* **5,** 1325–1338
46. Schweigerer, L., Neufeld, G., Friedman, J., Abraham, J. A., Fiddes, J. C., and Gospodarowicz, D. (1987) *Nature* **325,** 257–259
47. Shinkaruk, S., Bayle, M., Lain, G., and Deleris, G. (2003) *Curr. Med. Chem. Anti-Canc. Agents* **3,** 95–117
48. McInnes, C., Kondejewski, L. H., Hodges, R. S., and Sykes, B. D. (2000) *J. Biol. Chem.* **275,** 14287–14294
49. Gibbs, A. C., Kondejewski, L. H., Gronwald, W., Nip, A. M., Hodges, R. S., Sykes, B. D., and Wishart, D. S. (1998) *Nat. Struct. Biol.* **5,** 284–288
50. Waltenberger, J., Claesson-Welsh, L., Siegbahn, A., Shibuya, M., and Heldin, C. H. (1994) *J. Biol. Chem.* **269,** 26988–26995
51. Leenders, W., Lubsen, N., van Altena, M., Clauss, M., Deckers, M., Lowik, C., Breier, G., Ruiter, D., and de Waal, R. (2002) *Lab. Invest.* **82,** 473–481
52. Stacker, S. A., Vitali, A., Caesar, C., Domagala, T., Groenen, L. C., Nice, E., Achen, M. G., and Wilks, A. F. (1999) *J. Biol. Chem.* **274,** 34884–34892
53. Seghezzi, G., Patel, S., Ren, C. J., Gualandris, A., Pintucci, G., Robbins, E. S., Shapiro, R. L., Galloway, A. C., Rifkin, D. B., and Mignatti, P. (1998) *J. Cell Biol.* **141,** 1659–1673
54. Asahara, T., Bauters, C., Zheng, L. P., Takeshita, S., Bunting, S., Ferrara, N., Symes, J. F., and Isner, J. M. (1995) *Circulation* **92,** 365–371
55. Compagni, A., Wilgenbus, P., Impagnatiello, M. A., Cotten, M., and Christofori, G. (2000) *Cancer Res.* **60,** 7163–7169
56. Ke, L. D., Shi, Y. X., Im, S. A., Chen, X., and Yung, W. K. (2000) *Clin. Cancer Res.* **6,** 2562–2572
57. Sasisekharan, R., Shriver, Z., Venkataraman, G., and Narayanasami, U. (2002) *Nat. Rev. Cancer* **2,** 521–528
58. Iozzo, R. V., and San Antonio, J. D. (2001) *J. Clin. Invest.* **108,** 349–355
59. Kroll, J., and Waltenberger, J. (1997) *J. Biol. Chem.* **272,** 32521–32527
60. Namiki, A., Brogi, E., Kearney, M., Kim, E. A., Wu, T., Couffinhal, T., Varticovski, L., and Isner, J. M. (1995) *J. Biol. Chem.* **270,** 31189–31195
61. Park, J. E., Keller, G. A., and Ferrara, N. (1993) *Mol. Biol. Cell* **4,** 1317–1326
62. Wilting, J., Christ, B., and Weich, H. A. (1992) *Anat. Embryol.* **186,** 251–257
63. Friedlander, M., Brooks, P. C., Shaffer, R. W., Kincaid, C. M., Varner, J. A., and Cheresh, D. A. (1995) *Science* **270,** 1500–1502
64. Avgeropoulos, N. G., and Batchelor, T. T. (1999) *Oncologist* **4,** 209–224
65. Plate, K. H., Breier, G., Weich, H. A., and Risau, W. (1992) *Nature* **359,** 845–848
66. O'Reilly, M. S., Boehm, T., Shing, Y., Fukai, N., Vasios, G., Lane, W. S., Flynn, E., Birkhead, J. R., Olsen, B. R., and Folkman, J. (1997) *Cell* **88,** 277–285
67. O'Reilly, M. S., Holmgren, L., Shing, Y., Chen, C., Rosenthal, R. A., Moses, M., Lane, W. S., Cao, Y., Sage, E. H., and Folkman, J. (1994) *Cell* **79,** 315–328

Structure and Inhibitory Effects on Angiogenesis and Tumor Development of a New Vascular Endothelial Growth Inhibitor

Lior Zilberberg, Svetlana Shinkaruk, Olivier Lequin, Benoit Rousseau, Martin Hagedorn, Francesco Costa, Dario Caronzolo, Maurice Balke, Xavier Canron, Odile Convert, Georges Laïn, Karine Gionnet, Mario Gonçalvès, Mireille Bayle, Lorenzo Bello, Gerard Chassaing, Gérard Deleris and Andreas Bikfalvi

J. Biol. Chem. 2003, 278:35564-35573.
doi: 10.1074/jbc.M304435200 originally published online July 1, 2003
